Design and implementation of a robust and cost-effective double-scattering system at a horizontal proton beamline

Helmbrecht, S.; Baumann, M.; Fiedler, F.; Enghardt, W.; Krause, M.; Lühr, A.;

Originally published:

November 2016

Journal of Instrumentation 11(2016), T11001

DOI: https://doi.org/10.1088/1748-0221/11/11/T11001

A robust and cost-effective proton double-scattering system for experimental purposes

Ein robustes und kostengünstiges Doppelstreusystem für Protonenexperimente

Stephan Helmbrecht[a,b], Michael Baumann[a,c,d,e], Wolfgang Enghardt[a,c,d,e], Fine Fiedler[b], Mechthild Krause[a,c,d,e], Armin Lühr[a,c,e]

[a] *OncoRay – National Center for Radiation Research in Oncology, Faculty of Medicine and University Hospital Carl Gustav Carus, Technische Universität Dresden and Helmholtz-Zentrum Dresden-Rossendorf, Germany*
[b] *Helmholtz-Zentrum Dresden-Rossendorf, Institute of Radiation Physics, Dresden, Germany*
[c] *German Cancer Consortium (DKTK), Dresden, Germany and German Cancer Research Center (DKFZ), Heidelberg, Germany*
[d] *Department of Radiation Oncology, University Hospital Carl Gustav Carus, Technische Universität Dresden, Dresden, Germany*
[e] *Helmholtz-Zentrum Dresden-Rossendorf, Institute of Radiooncology, Dresden, Germany*

Abstract

Purpose: With an increasing number of proton therapy facilities coming into operation, also the interest for research at proton beams increases. Though many centers provide beam at an experimental room, some of these rooms do not feature a device for radiation field shaping, a so called nozzle. Therefore, a robust, mobile, and cost-effective double-scattering system for horizontal proton beamlines has been designed and implemented.

Materials and methods: The nozzle is based on the double scattering technique. Two lead scatterers, an aluminum ridge-filter and two brass collimators were optimized in a simulation study to form a laterally homogeneous 10 cm × 10 cm field with a spread-out Bragg-peak (SOBP). The parts were mainly manufactured using 3D printing techniques and the system was set up at the experimental beamline of the University Proton Therapy Dresden (UPTD). Measurements of the radiation field were carried out using a water phantom.

Results: High levels of dose homogeneity were found in lateral (dose variation $\Delta D < \pm 2\%$) as well as in beam direction ($\Delta D < \pm 3\%$ in the SOBP). The system has already been used for radiobiology and physical experiments.

Conclusion: The presented setup allows for creating clinically realistic extended radiation fields at fixed horizontal proton beamlines and is ready to use for internal and external users. The excellent performance combined with the simplistic design let it appear as a valuable option for proton therapy centers intending to foster their experimental portfolio.

Zusammenfassung

Ziel: Mit einer steigenden Zahl sich in Betrieb befindlicher Protonentherapieanlagen steigt auch das Interesse an Forschung mit Protonenstrahlen. Zwar besitzen viele Zentren einen Experimentierraum mit Protonenstrahl, jedoch gibt es einige davon, die ohne eine Vorrichtung zur Strahlformierung – eine sogenannte Nozzle – ausgestattet sind. Daher wurde ein robustes, mobiles und kostengünstiges Doppelstreusystem für horizontale Protonenstrahlführungen konzipiert und implementiert.

Material und Methoden: Die Nozzle basiert auf der Doppelstreutechnik. Zwei Streuer aus Blei, ein Ridge-Filter aus Aluminium und zwei Kollimatoren aus Messing wurden zunchst in einer Simulationsstudie

optimiert, um lateral homogene 10 cm × 10 cm Felder mit einem in Strahlrichtung ausgedehnten Bragg-Peak (SOBP) zu formen. Das System wurde an der experimentellen Strahlführung der Universitäts Protonen Therapie Dresden (UPTD) aufgestellt. Die Teile wurden hauptsächlich mittels der 3D-Druck-Technik hergestellt. Messungen des Strahlenfeldes wurden unter Nutzung eines Wasserphantoms durchgeführt.

Ergebnisse: Das System erreicht ein durch Messungen bestätigtes hohes Maß an Dosishomogenität sowohl in lateraler (Dosisvariation $\Delta D < \pm 2\%$) als auch in Strahlrichtung ($\Delta D < \pm 3\%$ im SOBP). Das System wurde bereits für strahlenbiologische und physikalische Experimente verwendet.

Schlussfolgerung: Der präsentierte Aufbau ermöglicht klinisch realistische ausgedehnte Strahlenfelder an horizontalen Protonenstrahlführungen und ist für interne und externe Anwender verfgbar. Die exzellente Leistungsfähigkeit kombiniert mit dem einfachen Design lassen diese Lösung als wertvolle Option für Protonentherapiezentren erscheinen, die beabsichtigen ihr experimentelles Portfolio zu stärken.

Keywords:
radiation field formation, radiobiology, ion beam therapy, proton therapy
Strahlfeldformierung, Strahlenbiologie, Ionenstrahltherapie, Protonentherapie

1. Introduction

Particle therapy has the potential to improve radiotherapy due to its higher spatial dose conformity and biological effectiveness compared to photon irradiation. At the same time, full utilization of these advantages requires advanced capabilities regarding high-precision delivery and monitoring of dose and a profound understanding of the variability of the relative biological effectiveness (RBE) for different beam qualities and cells [1, 2]. Accordingly, considerable effort is put on research to enhance particle therapy.

While at particle therapy centers patient treatment is usually prioritized, several centers also provide an experimental or quality assurance (QA) room with a beamline available for particle therapy experiments. However, for some of these rooms field formation capabilities are insufficient to meet requirements for clinically relevant experiments. For example, the large experimental room at the University Proton Therapy Dresden (UPTD) has been set up with a fixed horizontal beam line without the capability to create laterally extended radiation fields. To perform experimental proton radiobiology campaigns, a device to form treatment fields comparable to clinical conditions had to be installed meeting several specifications. First, mounting and demounting of the device at the beam line before and after a dedicated experiment has to be fast and reproducible. Accordingly, mobility, compactness, and robustness are essential. Second, design and production should be time- and cost-effective and realized in a way that makes it also convenient for other centers to (re-)build a comparable device when necessary.

In this work, we present the design and setup of a dedicated mobile proton double scattering beam shaping device as is now available for experiments at the UPTD for internal and external users. Additionally, we show its measured performance to demonstrate the ability to form proton fields relevant for radiobiology and physics experiments.

2. Materials and Methods

2.1. Design of scattering nozzle

A formalism by Takada [3] for a dual-ring double scattering method for proton beam spreading was used as starting point to determine optimal design parameters for the double scattering nozzle. The following specifications served as input for the nozzle design:

1. lateral dose homogeneity in an area of 10 cm × 10 cm,

*Corresponding author
Email address: armin.luehr@oncoray.de (Armin Lühr)

2. spread-out Bragg-peak (SOBP) width of about 3 cm,
3. low neutron load in the target volume, and
4. possibility to shape lateral dose contours,
5. maximal total length of the nozzle setup of 150 cm (restricted by available space at the beamline),
6. simplicity of design (especially no moving parts).

To achieve the aforementioned objectives (in particular item 6) it was decided to radically reduce the parameter space by using only a single primary energy $E_p = 150\,\mathrm{MeV}$. The dimensions of all nozzle components were calculated by means of a dedicated software written in Python based on the parameters obtained with the Takada formalism. Specifically, the software translates the required scattering angles and proton stopping into material extensions by using Highland's formula [4] and stopping power tables [5], respectively.

Figure 1 (upper row) shows a scheme of the setup. The beam enters the first scatterer (SC_1), which consists of a single lead foil to widen the lateral proton distribution. The second scatterer (SC_2) is a dual ring scatterer which is built from a lead foil covering the full beam radius and a thicker central (with smaller diameter) lead foil. SC_2 flattens the lateral fluence distribution, which is no longer Gaussian when leaving SC_2. To compensate for the different energy loss in the inner and outer part of SC_2 caused by the different thicknesses of the foils, a compensator made from polymethyl methacrylate (PMMA) is applied. To obtain an SOBP with a homogeneous dose region, a one dimensional ridge-filter is placed downstream. Its properties were calculated using the approach by Bortfeld and Schlegel [6] and formulas by Jette and Chen [7]. To cut the radiation field laterally, two collimators are applied. While a single collimator would be sufficient to stop protons with an energy lower than 150 MeV, the primary function of the first collimator is to considerably reduce the neutron contamination in the target volume as shown in figure 1. The fabrication of the nozzle elements is described in detail in section 2.3.

2.2. Monte Carlo Simulation

A Monte Carlo simulation of the nozzle has been setup using SHIELD-HIT12A [8, 9] to achieve three goals: a) optimization and fine tuning of beam shaping elements, b) *in silico* verification of nozzle design, and c) simulation of radiation field as basis for a beam model.

Two different scorer arrangements were used covering either the whole setup or only the target volume distal to the second collimator. The former had a relatively coarse spatial resolution of $10 \times 10 \times 10\,\mathrm{mm}^3$ and the latter a high resolution of $2 \times 2 \times 1\,\mathrm{mm}^3$ (1 mm in beam direction). The quantities dose, particle fluence, and linear energy transfer (LET) were scored for the total radiation field as well as differential for specific particle species. To estimate the proton efficiency (ratio of protons entering the first scatterer and the target region) proton numbers were counted by plane scorers.

2.3. Fabrication of nozzle elements

All elements of the nozzle are mounted on a 95 mm rail system by Thorlabs[1] to ensure lateral alignment. All holders are adjustable in height. Commercially available mounting accessories were combined with customized holders for all nozzle elements. The latter holders were made of plastic using the 3D-printing technique to ensure a fast, cost-effective and custom-fit production of these parts. Plastic components also have the advantage of relatively fast decaying activity created during irradiation.

Scattering foils were made of high purity (99.95%) lead delivered by Goodfellow[2]. For the dual-ring second scatterer, the necessary energy compensator for the outer ring was made of PMMA (density $\rho = 1.19\,\mathrm{g\,cm^{-3}}$). The collimators were machined at the proton therapy workshop in exactly the same way as the apertures for patient treatment in double scattering mode. The material is brass type Cu58Zn39Pb3 with a density $\rho = 8.5\,\mathrm{g\,cm^{-3}}$.

The most complex part is the ridge filter, figure 2(a). It consists of 24 ridges each having a width of 5 mm and a maximal height of 13.73 mm. A single ridge is divided in 50 steps, figure 2(b), each having an

[1] Thorlabs Inc, Newton, New Jersey, USA
[2] Goodfellow GmbH, Bad Nauheim, Germany

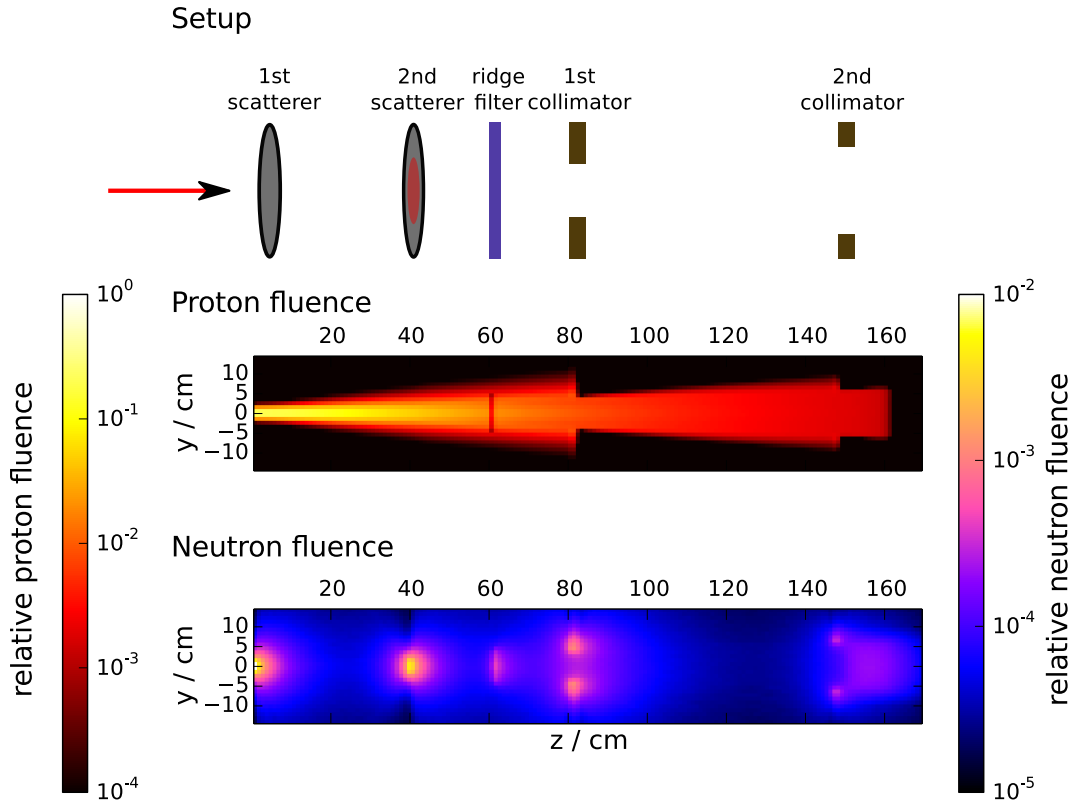

Figure 1: Schematic setup of the double scattering system along with simulated proton and neutron fluences in a central plane along the beam direction (z axis). The quantities are normalized to the number of incident protons. The effect of scatterers, collimators and the ridge-filter is, on the one hand, the shaping of the proton beam and, on the other hand, the creation of secondary radiation.

optimized step width proportional to the weight of the resulting Bragg-peak in the SOBP. The ridge-filter was manufactured of aluminum ($\rho = 2.7\,\mathrm{g\,cm^{-3}}$) using the 3D-printing technique selective Laser sintering by techno-plastic[3].

2.4. Measurement and analysis of dose distribution

The beamline at the experimental room of UPTD provides a proton beam with an energy $70 \leq E_\mathrm{p} \leq 230\,\mathrm{MeV}$. The lateral beam width is approximately $\sigma = 6\,\mathrm{mm}$ at the beam exit window. The maximal available beam current depends on the selected energy and is largest at high energies with a maximum of 30 nA [10]. A detailed analysis of the beam properties can be found in [11].

Relative and absolute dose measurements were carried out in a water phantom (type BluePhantom[4]) guided by the TRS 398 protocol [12] using PTW[5] advanced Markus (type 34045) and Semiflex (type 31010) ionization chambers, respectively, to analyze the achievable dose homogeneity in the target region. Due the mechanics of the phantom the ionization chambers could not directly be positioned at the inner phantom wall and an absolute depth position had to be determined. Therefore, a spacer of known thickness was placed between the phantom wall and the chamber during phantom setup. The water equivalent depth of this chamber position was determined as the sum of the water equivalent thickness (WET) of the phantom

[3]techno-plastic, Formenbau und Kunststoffverarbeitung GmbH, Sulzfeld, Germany
[4]iba Dosimetry GmbH, Bahnhofstrasse 5, 90592 Schwarzenbruck, Germany
[5]PTW-Freiburg, Physikalisch-Technische Werkstätten Dr. Pychlau GmbH, Lörracher Str. 7 79115 Freiburg, Germany

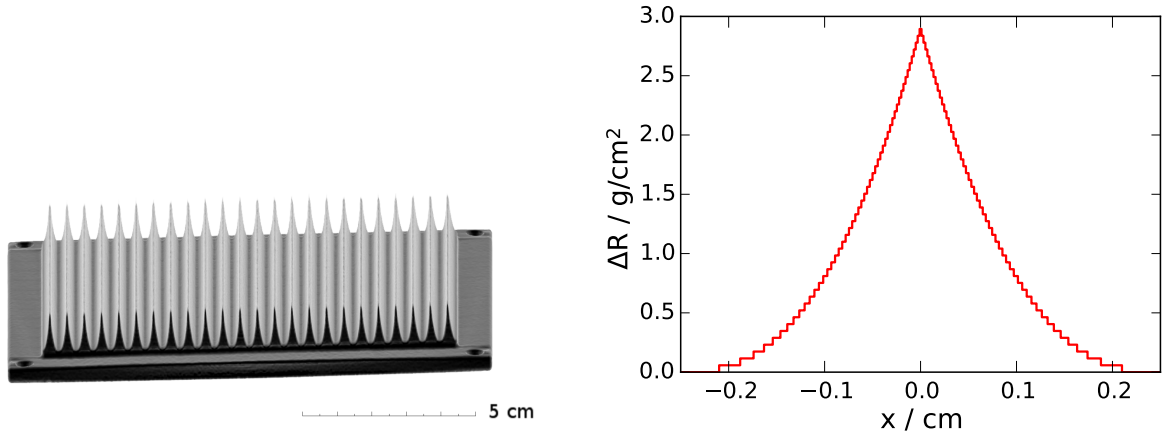

(a) CT image of manufactured ridge-filter

(b) Geometry of a single ridge

Figure 2: (b) Water equivalent thickness of a single element of the ridge filter. (a) Computed tomography image of the ridge filter acquired using a Siemens Somatom Sensation Open device. Image reconstruction was carried out using a protocol optimized for teeth imaging. The colors were inverted to visibility reasons.

wall (17.16 mm), the spacer thickness and the WET of the entrance window of the advanced Markus chamber (1.06 mm).

The desired homogeneous lateral dose plateau P had a width of $a = 10\,\mathrm{cm}$ centered at the midpoint between the lateral 50% dose points. Normalization was done by dividing the lateral dose distribution by the mean value of P. The distances between the lateral 50% and 90% dose levels were considered as the two widths W_{50} and W_{90}, respectively. A linear fit, F_l, with slope parameter, s_l, was applied to the measured dose in the plateau region P for quantitative evaluation.

The depth dose distributions were normalized as follows: First, the curve was normalized to its maximum. Second, the interval was selected, in which the dose was greater or equal 95%. From this interval, the proximal and distal quarters were subtracted. Third, the curve was normalized to the mean of the aforementioned remaining central interval. The ranges R_{50} and R_{90} were defined as the depths of the distal 50% and 90% dose level, respectively. The distance between the proximal and distal 95% dose level was considered as the modulation width M of the SOBP. Similar to the lateral evaluation, linear fits F_d and F_f were used to quantify the slope s_d within the SOBP region and s_f of the distal fall-off. F_d was applied to a region, which was half the modulation M wide and centered within the SOBP, and F_f was applied between the distal 80% and 20% dose.

3. Results

3.1. Simulation and optimization

Figure 3 shows the profiles through the dose distribution obtained in the simulation study. Though statistical fluctuations are visible in the lateral and horizontal profiles, an acceptable dose distribution was obtained.

3.2. Implementation and setup of nozzle

The double-scattering nozzle was set up as shown in figure 4. A table specifying detailed measures of the beam-shaping nozzle elements can be found in Appendix A. The lower part of figure 1 visualizes the effect of the beam shaping elements in terms of proton and neutron fluences as simulated by SHIELD-HIT12A. Here, also the role of the first collimator is illustrated, namely, to keep unnecessary proton fluence away from the second collimator and, hence, lower the neutron production in the proximity of the target region.

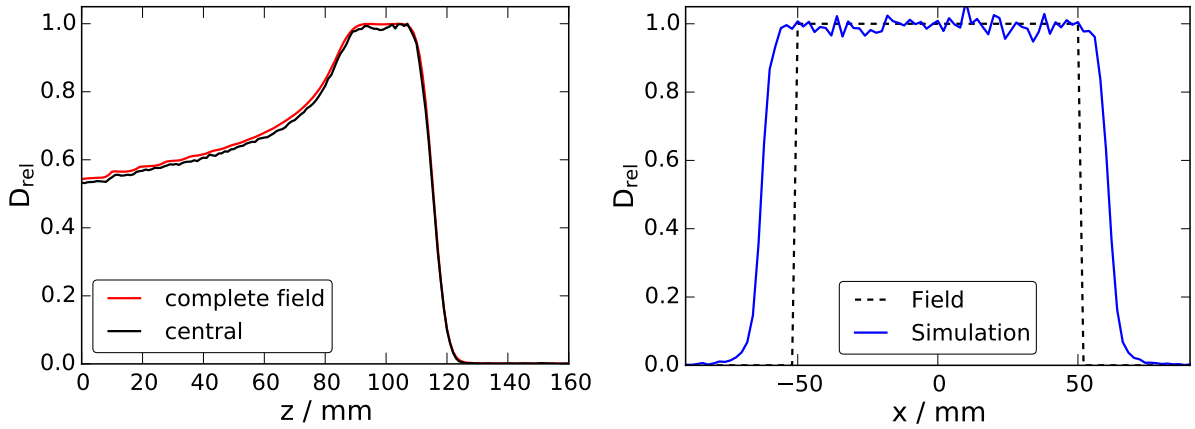

(a) Simulated depth dose dependency

(b) Simulated lateral dose profile

Figure 3: (a) Depth dose profiles obtained in the Monte Carlo simulation. Red line: dose averaged over the desired lateral field width; black line: dose along the central beam axis. (b) Simulated lateral dose distribution in the SOBP (100 mm depth). The dashed line shows the desired field extension.

The simulations revealed a relatively high efficiency of the design with 30% of all protons entering the setup also finally reach the homogeneous target region.

Prior to any proton experiment that required the nozzle, the latter had to be mounted in front of the exit of the proton beam line and removed afterward. As a first step, the rail system supporting the nozzle elements was adjusted relative to a positioning laser. Second, by using the Lynx[6] detector for 2D dose acquisition, the nozzle elements were conveniently aligned with the proton beam axis with sub-millimeter accuracy in less than an hour. Thereby, a high degree of dose homogeneity could be ensured each time the system was set up.

3.3. Lateral dose distribution

Measurements of the lateral dose distribution were performed for different settings of the ridge-filter:

1. no ridge-filter in place
2. ridge-filter with $\alpha = 0°$
3. ridge-filter with $\alpha = 45°$

where α denotes the angle between the beam axis and the normal vector of the base plane of the ridge-filter. Dose characteristics in lateral direction, both horizontally and vertically, are summarized in Tab. 1.

For settings 1 to 3 a linear dose increase of up to 0.03%/mm was observed in the lateral dose plateau, figure 5(a). Such a tilt is a result of a slight misalignment of the second scatterer. Therefore, an additional measurement was carried out after the optimization of the mounting of the scatterer, referred to as setting 4. Using this refinement a high level of dose homogeneity could be achieved in lateral direction, figure 5(b), with a variation of dose $\leq 1\%$ within the desired field size of $10 \times 10\,\mathrm{cm}^2$. It should be noted, that the width is (intentionally) greater than the minimally desired homogeneous field width of $10 \times 10\,\mathrm{cm}^2$. The openings of the collimators have been manufactured with an extra margin to avoid a decrease in dose at the edges when irradiating cell probes.

[6]iba Dosimetry GmbH, Bahnhofstrasse 5, 90592 Schwarzenbruck, Germany

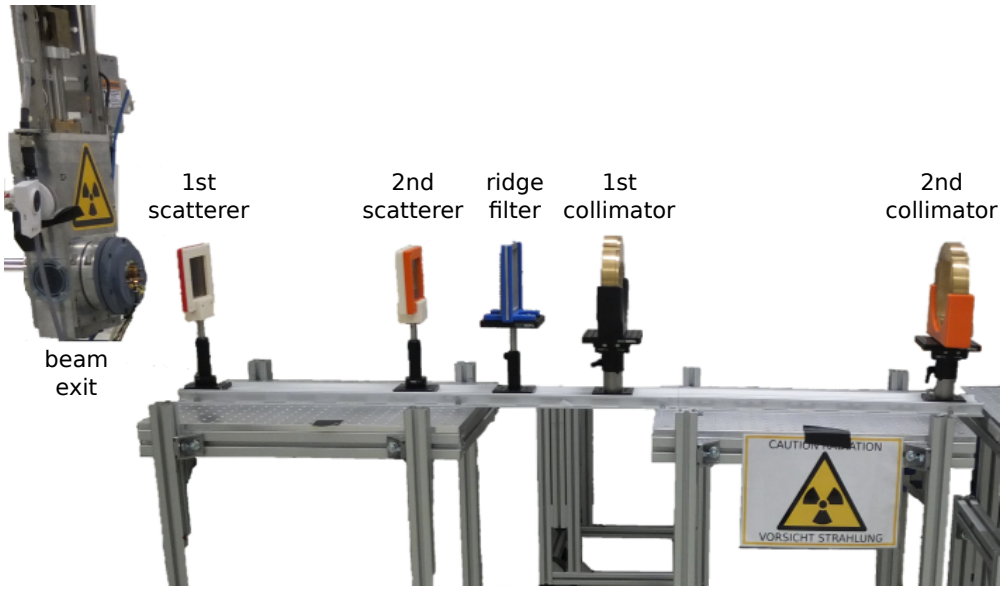

Figure 4: Complete setup of the scattering system with the two scatterers, the ridge-filter, and the two collimators.

Table 1: Characterization of radiation field in the lateral directions at a water-equivalent depth of 77 mm and 112 mm for settings 1-3 and setting 4, respectively. Dose given in %.

#	Setting	W_{50}/ mm	W_{90}/ mm	STD(D_p)	min(D_p)	max(D_p)	s_l/ %/mm
Horizontal (x)							
1	no RiFi	129	122	1	98	103	0.016
2	RiFi $\alpha = 0°$	129	121	1	99	102	0.013
3	RiFi $\alpha = 45°$	129	119	1	97	101	0.021
4	after adjustment	129	119	1	99	101	0.019
Vertical (y)							
2	RiFi $\alpha = 0°$	130	120	1	98	103	0.031
3	RiFi $\alpha = 45°$	130	122	1	97	103	0.005
4	after adjustment	129	118	0	99	101	0.000

RiFi: ridge-filter; STD: standard deviation; D_p: dose distribution in plateau; s_l: lateral slope

3.4. Depth-dose distribution

Depth-dose curves were measured for the same three settings of the ridge-filter as for the lateral case. Dose characteristics of the depth-dose profile are summarized in Tab. 2. For settings 1 and 2, measured depth-dose distributions are shown in Fig. 6. By rotation of the ridge-filter from 0 to 45 degrees (cf. [13] for details), it was possible to (continuously) increase the modulation width M of the SOBP from 19.9 mm to 31.9 mm. A high level of dose homogeneity within the central SOBP was found with only a small slope toward the distal end. The ridge-filter reduced the ranges and the steepness of the distal fall-off of the SOBPs in comparison to the pristine Bragg peak.

3.5. Customization for different experiments

Depending on the demands of a specific experiment, the scattering setup can be further customized: Range compensators can be inserted up- or downstream the second collimator to adjust the particle energy. To create more complex radiation fields, customized collimators – just as apertures for patient treatment – can be inserted in the holder of the second collimator. Such a setup has, e.g., be used for an in-beam PET experiment [14].

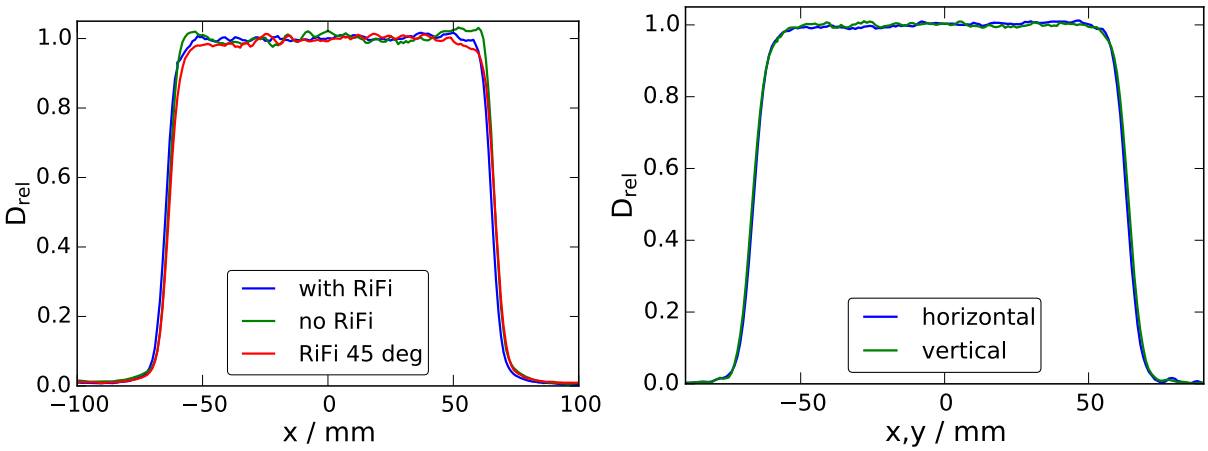

(a) Horizontal dose distributions (settings 1-3)

(b) Lateral dose distributions (setting 4)

Figure 5: Measured lateral dose distributions. (a) Horizontal dose profiles with different settings of the ridge filter at a water equivalent depth of 77 mm. (b) Lateral dose profiles after refinement of the positioning of the second scatterer in the depth of the SOBP (112 mm).

Table 2: Characteristic measures of the depth-dose distributions. Dose given in %.

#	Setting	R_{50}/ mm	R_{90}/ mm	M/ mm	s_{d}/ %/mm	s_{f}/ %/mm
1	no RiFi	125.5	123.0	–	–	-18
2	RiFi $\alpha = 0°$	119.4	115.8	19.9	0.077	-13
3	RiFi $\alpha = 45°$	117.3	113.6	31.9	0.038	-13

RiFi: ridge-filter; s_d: slope within SOBP; s_f: slope of distal fall-off

Absolute dosimetry is performed as in clinical operation. The dose measured by a sensor in the radiation field, e.g. an ionization chamber or film, is correlated to the charge acquired by the transmission chamber at the beam exit. This procedure yields a number of so called monitor units, required to deliver the desired dose. Absolute dose as function of MU should be determined prior to an experiment to verify the stability of this relation on a daily basis as part of a QA procedure. The control system at the experimental beamline of UPTD allows also for a direct connection of a PTW[7] Unidos electrometer, to switch the beam off when a certain dose has been reached.

4. Discussion

We present a design of a mobile, robust, and cost-effective double scattering proton nozzle prototype that is useful to produce clinically relevant homogeneous dose distributions at horizontal proton beamlines. The radiation field specifications were verified by extensive dose measurements showing a high degree of dose homogeneity in lateral (10 cm × 10 cm) directions at all depths down to the distal edge and, when applying a ridge-filter, also in longitudinal direction. The mobility and reproducibility of the setup allows for switching between pencil beam and extended field irradiation in double scattering mode at the experimental beamline.

Other double scattering solutions, such as a contoured second scatterer [15], have been proposed. We employed the dual ring approach primarily because of its low complexity and potentially higher robustness. In general, the most critical point of the nozzle setup turned out be the alignment of the nozzle with the proton beam axis and in particular the symmetric positioning of the second scatterer. However, the

[7]PTW-Freiburg, Germany

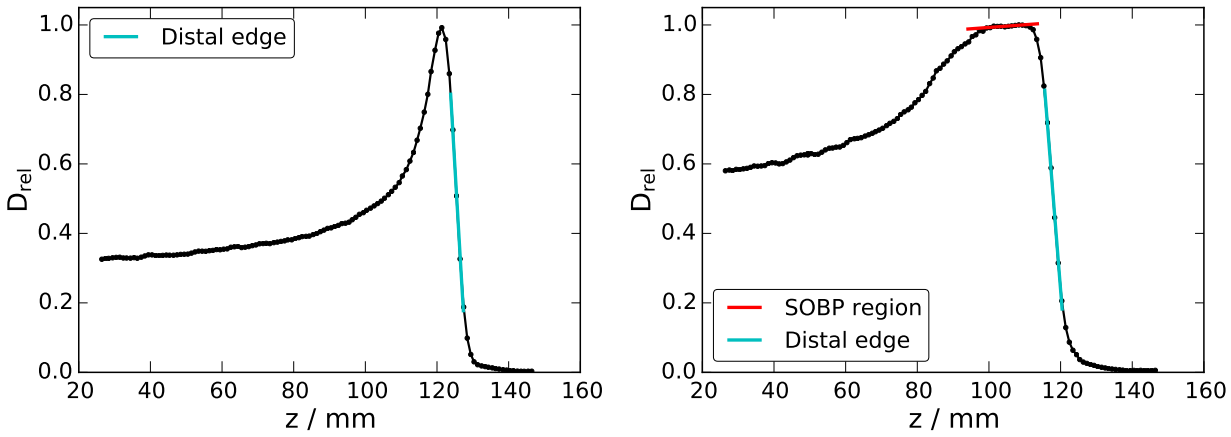

(a) Bragg peak without ridge-filter

(b) SOBP obtained with ridge-filter

Figure 6: Depth-dose distributions of the double-scattering setup acquired by means of a water phantom measured (a) without (setting 1) and (b) with (setting 2) ridge-filter. Linear fits were applied to the distal fall-off, F_f, and the central SOBP region, F_d. Black bullets: dose measurement; cyan solid line: fit F_f; red solid line: fit F_d.

alignment can be fast and conveniently performed using a 2D-dose measuring device – such as the Lynx in our case – until a homogeneous dose distribution is obtained along both orthogonal lateral directions. Since an asymmetry of the lateral dose distribution is directly related to a misalignment of the second scatterer, the adjustment was found to be straightforward.

Due to the requirements regarding mobility and robustness we abandoned any moving parts from the nozzle design. In particular, we favored a ridge-filter over a rotating range modulator wheel to produce spread-out Bragg peaks. The ridge-filter produced by convenient 3D-printing of aluminum showed a comparable performance as by demanding micro fabrication [16]. It was discussed, based on a Monte Carlo study, whether to use PMMA as ridge-filter material instead of the standard aluminum to reduce the number of those secondary neutrons in the target region by about 25% that originate from the ridge-filter [17]. However, based on the Monte Carlo simulations of the presented setup the main sources of neutrons are the scattering foils and the primary collimator made of lead and brass, respectively. Essentially, it is the function of the primary collimator to stop most of the protons that will otherwise hit the main collimator to reduce the load of secondary radiation in the target volume. Due to the same aim, a proton efficiency of about 30% was envisaged despite the compact nozzle design and without compromising the dose homogeneity in the entire target volume.

The close vicinity of lead and brass parts to the target area may cause radiation protection issues. After approximately 8 hours of experiments, local dose rates of up to 500 μSv/h were measured in 10 cm distance to the lead scatterers. While most of the radiation components decay within hours or days, the dose rates need to be carefully evaluated and should be considered when planning experimental workflows.

In its current state, the designed nozzle can be set up prior to proton radiation experiments requiring an extended homogeneous field. So far, it has been used for a whole range of different experiments regarding (*in vivo*) proton range verification measurements and radiobiological cell irradiation experiments. In vivo mouse irradiation of xenograft models is in preparation.

Currently, irradiation of small animals with orthotopic tumors receives a lot of attention in the radiotherapy community. Such irradiations are performed using, e.g., dedicated small animal devices integrating X-ray imaging and irradiation [18, 19]. We plan to apply the concept described in this paper also for setting up a specific proton irradiation site for small animals using an industrial robot, which is installed above the beam line for positioning based on previous small animal imaging.

5. Conclusion

Extended proton radiation fields are required for physics and radiobiology experiments in translational cancer research. A double-scattering and double-collimating system has been designed and built, that provides homogeneous extended treatment fields at fixed horizontal proton beams.

The system has already proven its usability in different experiment campaigns and is now available for internal as well as external users. The design is also interesting for other centers equipped with an experimental beamline with a need for beam formation. Especially, the application of the latest manufacturing techniques like 3D printing of plastics and metals allows for rapid, convenient and cost-effective implementation.

Acknowledgments

The construction and supervision of manufacturing of the components by Anne Dreyer, Institute of Radiooncology, Helmholtz-Zentrum Dresden-Rossendorf, is gratefully acknowledged by the authors. We kindly thank Partick Wohlfahrt, M.Sc., for the CT imaging of the ridge-filter.

References

[1] O. Jäkel, The relative biological effectiveness of proton and ion beams, Z. Med. Phys. 18 (4) (2008) 276–285. doi:10.1016/j.zemedi.2008.06.012.
URL http://www.sciencedirect.com/science/article/pii/S0939388908000822

[2] H. Paganetti, Relative biological effectiveness (RBE) values for proton beam therapy. variations as a function of biological endpoint, dose, and linear energy transfer, Phys. Med. Biol. 59 (22) (2014) R419.
URL http://stacks.iop.org/0031-9155/59/i=22/a=R419

[3] Y. Takada, Dual-ring double scattering method for proton beam spreading, Jpn. J. Appl. Phys. 33 (1R) (1994) 353.

[4] V. Highland, Some practical remarks on multiple scattering, Nucl. Instr. Meth. 129 (2) (1975) 497–499.

[5] A. Lühr, J. Toftegaard, I. Kantemiris, D. C. Hansen, N. Bassler, Stopping power for particle therapy: The generic library libdEdx and clinically relevant stopping-power ratios for light ions, Int. J. Radiat. Biol. 88 (1-2) (2012) 209–212. doi:10.3109/09553002.2011.595877.
URL http://www.tandfonline.com/doi/abs/10.3109/09553002.2011.595877

[6] T. Bortfeld, W. Schlegel, An analytical approximation of depth - dose distributions for therapeutic proton beams, Phys. Med. Biol. 41 (8) (1996) 1331.
URL http://stacks.iop.org/0031-9155/41/i=8/a=006

[7] D. Jette, W. Chen, Creating a spread-out bragg peak in proton beams, Phys. Med. Biol. 56 (11) (2011) N131.
URL http://stacks.iop.org/0031-9155/56/i=11/a=N01

[8] D. C. Hansen, A. Lühr, N. Sobolevsky, N. Bassler, Optimizing SHIELD-HIT for carbon ion treatment, Phys. Med. Biol. 57 (8) (2012) 2393.
URL http://stacks.iop.org/0031-9155/57/i=8/a=2393

[9] N. Bassler, D. C. Hansen, A. Lühr, B. Thomsen, J. B. Petersen, N. Sobolevsky, SHIELD-HIT12A - a Monte Carlo particle transport program for ion therapy research, Journal of Physics: Conference Series 489 (1) (2014) 012004.
URL http://stacks.iop.org/1742-6596/489/i=1/a=012004

[10] S. Helmbrecht, F. Fiedler, M. Meyer, P. Kaever, T. Kormoll, Proton beams for physics experiments at oncoray, Radiother. Oncol. 118, Supplement 1 (2016) S60 – S61, ICTR-PHE 2016, 15-19 February 2016, CICG, Geneva, Switzerland. doi:http://dx.doi.org/10.1016/S0167-8140(16)30124-4.
URL http://www.sciencedirect.com/science/article/pii/S0167814016301244

[11] J. Petzoldt, K. Roemer, W. Enghardt, F. Fiedler, C. Golnik, F. Hueso-Gonzalez, S. Helmbrecht, T. Kormoll, H. Rohling, J. Smeets, T. Werner, G. Pausch, Characterization of the microbunch time structure of proton pencil beams at a clinical treatment facility, Phys. Med. Biol. 61 (6) (2016) 2432.

[12] IAEA, Absorbed Dose Determination in External Beam Radiotherapy.
URL http://www-pub.iaea.org/books/IAEABooks/5954/Absorbed-Dose-Determination-in-External-Beam-Radiotherapy

[13] T. Nakagawa, K. Yoda, A method for achieving variable widths of the spread-out bragg peak using a ridge filter, Med. Phys. 27 (4) (2000) 712–715. doi:http://dx.doi.org/10.1118/1.598933.
URL http://scitation.aip.org/content/aapm/journal/medphys/27/4/10.1118/1.598933

[14] S. Helmbrecht, W. Enghardt, F. Fiedler, M. Iltzsche, G. Pausch, C. Tintori, T. Kormoll, In-beam pet at clinical proton beams with pile-up rejection, Z. Med. Phys. submitted.

[15] E. Grusell, A. Montelius, A. Brahme, G. Rikner, K. Russell, A general solution to charged particle beam flattening using an optimized dual-scattering-foil technique, with application to proton therapy beams, Phys. Med. Biol. 39 (12) (1994) 2201.
URL http://stacks.iop.org/0031-9155/39/i=12/a=005

[16] T. Akagi, A. Higashi, H. Tsugami, H. Sakamoto, Y. Masuda, Y. Hishikawa, Ridge filter design for proton therapy at Hyogo Ion Beam Medical Center, Phys. Med. Biol. 48 (22) (2003) N301. doi:10.1088/0031-9155/48/22/N01.
URL http://stacks.iop.org/0031-9155/48/i=22/a=N01

[17] Z. Riazi, H. Afarideh, R. Sadighi-Bonabi, Influence of ridge filter material on the beam efficiency and secondary neutron production in a proton therapy system, Z. Med. Phys. 22 (3) (2012) 231–240. doi:10.1016/j.zemedi.2012.06.001.
URL http://www.sciencedirect.com/science/article/pii/S0939388912000621

[18] F. Verhaegen, P. Granton, E. Tryggestad, Small animal radiotherapy research platforms, Physics in Medicine and Biology 56 (12) (2011) R55.
URL http://stacks.iop.org/0031-9155/56/i=12/a=R01

[19] F. Tillner, P. Thute, R. Bütof, M. Krause, W. Enghardt, Pre-clinical research in small animals using radiotherapy technology a bidirectional translational approach, Z. Med. Phys. 24 (4) (2014) 335–351. doi:10.1016/j.zemedi.2014.07.004.
URL http://www.sciencedirect.com/science/article/pii/S0939388914000956

Appendix A. Design parameters

Table A.3 shows relevant geometric measures necessary to rebuild the scattering system. The most critical measures are the thicknesses and positions of the lead foils. Note that, while lead is a soft metal which tends to deformation, a change in thickness is likely to cause a variation of the field shape.

Table A.3: Design parameters of the scattering system. Data have been measured where feasible. Otherwise, they origin from the engineering drawing or from the data sheet provided by the supplier.

Parameter	data source	Value
Scatterer 1 (SC_1):		
Position z	measurement	0.0 mm
Area	measurement	$81\times81\,\mathrm{mm}^2$
Thickness of lead foil	construction	3.1 mm
Scatterer 2 (SC_2):		
Position z	measurement	430.0 mm
Area	measurement	$81\times81\,\mathrm{mm}^2$
Thickness lead foil complete field	construction	0.7 mm
Thickness central lead foil	construction	3.3 mm
Diameter central lead foil	construction	37.4 mm
Thickness PMMA compensator	construction	17.1 mm
Ridge filter		
Position z	measurement	630.0 mm
Material	construction	Aluminum
Density	supplier	$2.7\,\mathrm{g\,cm}^{-3}$
Area	measurement	$120\times120\,\mathrm{mm}^2$
Thickness of base	measurement	3.0 mm
Maximum ridge thickness	measurement	13.4 mm
Number of ridges	measurement	24
Ridge orientation		horizontal
Angle ridges / beam		$0\ldots45°$
Collimator 1		
Position z	measurement	830.0 mm
Material	construction	Cu58Zn39Pb3
Density	supplier	$8.5\,\mathrm{g\,cm}^{-3}$
Thickness	measurement	33.0 mm
Area of opening	measurement	$77.5\times77.0\,\mathrm{mm}^2$
Collimator 2		
Position z	measurement	1500.0 mm
Material	construction	Cu58Zn39Pb3
Density	supplier	$8.5\,\mathrm{g\,cm}^{-3}$
Thickness	measurement	33.0 mm
Area of opening	measurement	$115.0\times115.5\,\mathrm{mm}^2$